Multi-functional groups decorated composite nanofiber separator with excellent chemical stability in ester-based electrolyte for enhancing the lithium-ion transport

Multi-functional groups decorated composite nanofiber separator with excellent chemical stability in ester-based electrolyte for enhancing the lithium-ion transport

*Xin Xie[a,1], Lei Sheng[a,b,1], Catia Arbizzani[b], Bin Gao[a], Xingxu Gao[a], Ling Yang[a], Yaozong Bai[c], Haoyu Dong[c], Gaojun Liu[c], Tao Wang[a], Xianli Huang[a], Jianping He[a]**

[1] These authors contributed equally to this work.

[a] College of Material Science and Technology, Nanjing University of Aeronautics and Astronautics, 210016, Nanjing, Jiangsu Province, China.

[b] Department of Chemistry "Giacomo Ciamician", University of Bologna, 40126, Bologna, Italy

[c] Sinoma Lithium Battery Separator Co. Ltd, 277500, ZaoZhuang, Shandong province, China

ABSTRACT

As various heat-resistant polymer separators come out, although they possess better thermal stability and superior affinity to liquid electrolyte than commercial polyolefin separator, the porous structure and chemical stability of these novel separators should be paid more attention. In this work, we prepare a thin polyacrylonitrile/cellulose acetate (PAN/CA) composite nanofiber separator and discuss the importance of chemical stability in the ester-based electrolyte. The addition of CA decreases the PAN/CA fiber diameter from 310 nm to 210 nm. However, CA containing a lot of ester groups is easy to be dissolved by liquid electrolyte for the property of similarity and compatibility. Hence, the obtained PAN/CA composite nanofiber separator is treated via alkaline hydrolysis process, and some ester groups are transformed to be hydroxyl groups. Noteworthily, hydroxyl-rich PAN/CA composite nanofiber separator not only remains stable in electrolyte, but also possesses an improved lithium-ion

transport property for reducing concentration polarization effect. As a result, the $LiCoO_2$/Li half cells employing the hydroxyl-rich composite nanofiber separator exhibits better capacity retention (118.5 mAh g^{-1} after 300 cycles) and superior rate performance (143.1 mAh g^{-1} at 3C). Therefore, this multi-functional groups decorated composite nanofiber separator with excellent chemical stability is a candidate for next-generation lithium-based battery.

***Keywords*:**

Nanofiber separator, chemical stability, multi-functional groups, battery performance.

*Corresponding author: *Jianping He*

Email address: jianph@nuaa.edu.cn;

1. Introduction

Since the industrial revolution started, fossil fuels have been consumed overmuch in the past two-hundred years, which is also gradually evolved as severe problems of environmental pollution and energy crisis [1]. It is time to develop clean and sustainable energy like solar, wind and hydropower [2-4]. However, these energy sources generally show the characteristics of discontinuity, regional and instability, which make it hard to be applied in most electronic device. Therefore, conversion and storage of energy have been the focus of new energy industrial. Lithium-ion battery (LIB) is one of the most competitive power supplies for high energy density and long cycle life, and it has been widely applied in portable electronics [5-10]. In recent years, when selected as the power supply, LIB safety issue becomes a core problem for electric vehicles (EVs) industrial [11]. It may be closely related to the LIB with high energy density [12]. Hence, more and more investigators are devoted to exploring novel materials and searching for a security design strategy about LIB.

Generally, a typical LIB consists of anode, cathode, separator and liquid electrolyte. Commercial liquid electrolyte is mainly composed of organic solvent and $LiPF_6$. The most used anode materials are divided into carbon-based materials, silica-based materials and alloy materials [13]. Li-insertion cathode materials besides traditional $LiCoO_2$ and $LiFePO_4$, some aqueous cathode materials have attracted more attention in recent years [14-16]. While separator mainly plays a significant part in isolating the anode and cathode [17]. Meantime, it could absorb enough electrolyte and provide special transport channels for lithium ions [18-20]. As an indispensable structural material inside the battery, separator should possess good chemical stability and thermal stability [17, 21]. At present, for the mature production process and low manufacturing cost, polyolefin microporous membrane with pore size of 20-300 nm is widely applied in LIB [22]. Nevertheless, this kind of polyolefin separator usually shows poor thermal stability [23-25] and it would shrink or even melt when the operating temperature closes to or exceeds the melting point [26]. Therefore, a large number of research about separators have been carried out to develop the safety performance of LIB at high temperature. The composite separator coated with inorganic ceramic particles (such as SiO_2 [27-29], Al_2O_3 [30-32], TiO_2 [33,34], ZrO_2 [35] and so on) has been successfully prepared and used in some occasions. For example, Park et al. selected poly (methyl methacrylate) as the binder and prepared a special kind of close-packed SiO_2/PMMA coating on PE separators. With the introduction of SiO_2 nanoparticles, thermal stability of composite separators was obviously improved, and the unique porous structure provided better electrolyte wettability and ionic transport ability [27]. Also, Liang et al. designed a unique nano-shield structure on the PE separator via the spinning process [36]. The results showed that neatly arranged SiO_2 nanoparticles could form uniform and dense lithium metal deposition, and the battery could stably cycle for more than 300 cycles. Furthermore, on the basis of ensuring the safety characteristics of LIB,

some conductive ceramic particles (such as LAGP [37], LATP [38], LLZO [39], etc.) were regarded as functional coating materials for separator in recent years. For instance, Liu et al. prepared a kind of LAGP layer coated composite separator with excellent wettability, chemical/thermal stability and mechanical strength. The composite separator effectively alleviated the contradiction between safety performance and electrochemical performance. Besides, Zhang et al. proposed an ion redistributor of LLZTO coated PP separator to regulate the transport process of lithium ions and supply a uniform lithium ions deposition in lithium-metal battery (LMB) [40]. Due to significant reduction of ion concentration standard deviation of LLZTO-coated PP separators, the Li/Cu cell exhibited a coulombic efficiency larger than 98% over 450 cycles.

On the other hand, some polymer materials (such as PI [41, 42], PVDF [43, 44] and so on) with great thermal stability and strong polarity are used as the separator in lithium-based batteries. Up to now, there are several methods that fabricate polymer porous membrane in recent years, such as TIPS, NIPS, electrospinning technology etc. For example, Cui et al. prepared a kind of composite separator based on PVDF, CA and $Al(OH)_3$ via NIPS [45]. The crystallinity of polymer matrix was decreased with the addition of $Al(OH)_3$. And the obtained separator exhibited excellent thermal stability and electrochemical performance. Wang et.al added single layer graphene oxide (GO) to PI spinning solution and prepared the GO/PI separator with smaller fiber diameter and enhanced porosity [46]. Compared with commercial separator, the GO/PI separator had an improved electrolyte uptake rate. In addition, Qi et al. also designed a new type of core-shell structure PI/SiO_2 inorganic-organic composite separator via SiO_2 nano-encapsulation [47]. This strategy combined the electrospinning technology and inorganic ceramic particles coating to effectively improve the safety performance and electrochemical performance.

Electrospinning technology is a very simple and efficient method, and the obtained nanofiber membrane has high porosity. For instance, it has been reported that the electrospinning nanofiber separators based on polyacrylonitrile (PAN) possess high electrolyte uptake [48, 49]. PAN is able to keep size stability below 317 ℃ and has good chemical stability [50, 51]. Furthermore, it is also reported that the polar nitrile groups of PAN may be in favor of transporting lithium ions [52, 53]. However, the self-discharge phenomenon of battery is closely associated with the pore size of nanofiber membrane, which needs to be controlled by hot-press or reduce the fiber diameter. Hence, it is a good method to adjust the fiber morphology by adding additives to the spinning precursor solution. In this study, we tried to prepare a thin PAN/cellulose acetate (CA) nanofiber membrane. CA, a kind of biodegradable polymer, is used as fiber morphology regulator [54]. And abundant ester groups of CA have good compatibility with liquid electrolyte and even could be dissolved by ester-based liquid electrolyte [55, 56]. Furthermore, after a simple alkaline hydrolysis treatment, PAN/CA composite nanofiber separator has a lot of hydroxyl groups, nitrile groups and unhydrolyzed ester groups, which make it stable in the ester-based liquid electrolyte and contribute to lithium-ion transport process.

2. Experimental

2.1 Materials

2-acrylonitrile homopolymer (PAN), cellulose acetate (CA), lithium hydroxide (LiOH) and N, N-dimethylformamide (DMF) were purchased from Aladding Reagent Co. Ltd. Ethanol and n-butanol were bought from Sinopharm Chemical Reagent Co. Ltd. Commercial carbonate-based electrolyte was purchased from DoDoChem. Lithium foil (diameter of 16 mm) was bought from China Energy Lithium Co. Ltd. Commercial lithium cobalt oxides ($LiCoO_2$) electrode and lithium iron phosphate

($LiFePO_4$) electrode were obtained from Guangdong Canrd Co. Ltd. Polyethylene separator (thickness of 16 μm) was kindly provided by Sinoma Lithium Battery Separator Co. Ltd. Deionized water was made in laboratory.

2.2 The preparation of PAN/CA composite separator

Firstly, 1.1 g PAN and 1.1 g CA were firstly added into 20 ml DMF, which were mixed under vigorously stirring for 12 h to prepare a homogeneous spinning solution (10.4%, w/w). Then the solution was put into two syringes. A stable and continuous Talor cone at the nozzle was expected to be formed by adjusting the spinning voltage, push speed and collected distance. Finally, nanofiber membrane was prepared under these conditions: humidity at 30%, temperature at 45 °C, push speed at 0.0010 mm s^{-1}, spinning voltage at 18 kV, and collected distance at 15 cm.

Next, the collected PAN/CA nanofiber membrane needed to evaporate the residual solvent at a vacuum drying oven for 24 h. Under the same experimental conditions, we set up three controlling groups (2.2 g pure PAN, 2.2 g pure CA, 0.55 g PAN+1.65 g CA, respectively, and the solvent was 20 ml DMF). And the corresponding electrospinning nanofiber membrane was prepared according to the same experimental procedure.

2.3 Alkaline hydrolysis treatment of PAN/CA composite nanofiber separator

1 g LiOH was firstly dissolved in 200 ml ethanol, and stirring for 30 minutes. Then the dried PAN/CA composite nanofiber separator was put into this solution and fully soaked for 12 h for alkaline hydrolysis treatment. After that, 0.01 mol L^{-1} hydrochloric acid solution was used to remove excess lithium salt dispersed in nanofiber separator. Finally, the obtained PAN/CA nanofiber separator was washed for three times with absolute ethanol and deionized water, respectively, and then dried in a preheated 70 °C vacuum drying box for 24 h. The entire preparation process of experimental materials

is displayed in **Figure 1**.

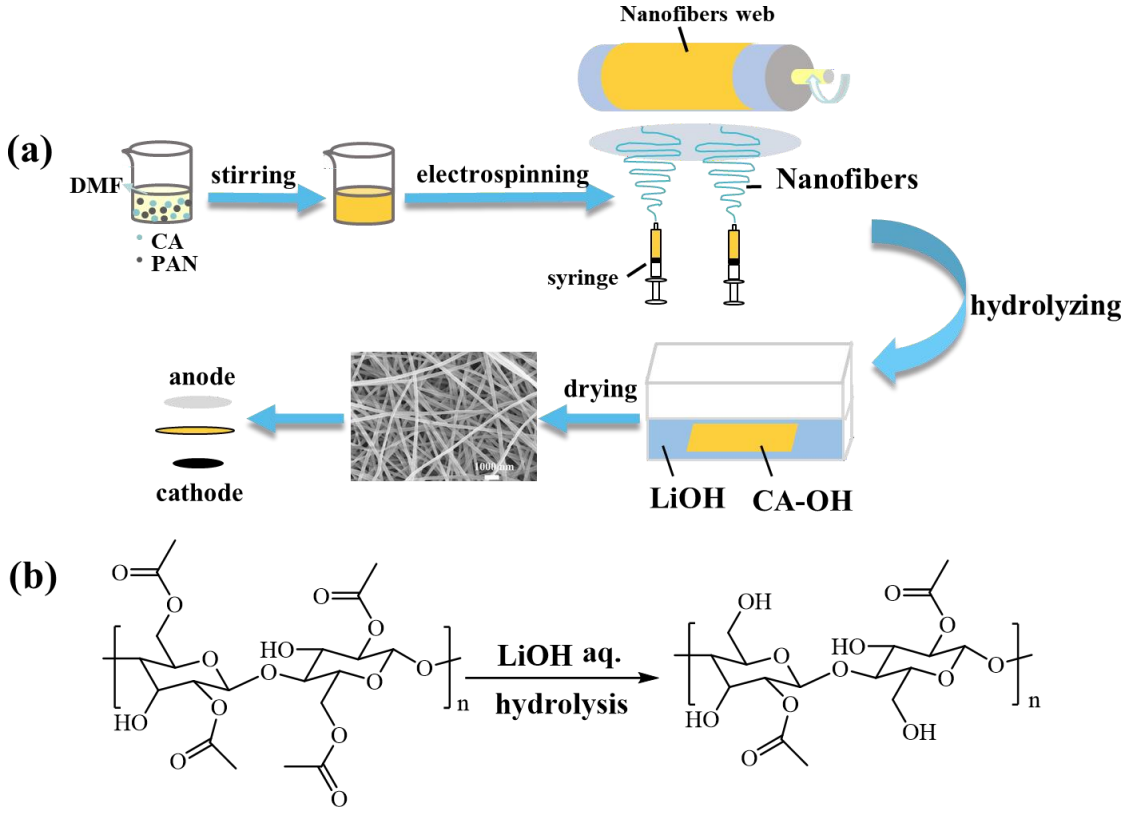

Figure 1. The schematics of preparation process (a) and alkaline hydrolysis process (b) of PAN/CA nanofiber separator.

2.4 Characterization of the separator

The surface morphology of nanofiber separators was observed by a scanning electron microscope (SEM, Japan, Hitachi, S-4800). High-resolution Transmission electron microscopy (HRTEM, FEI Tecnai G2F20) combined with energy dispersive X-ray spectroscopy (EDX) was used to study the matrix structure of nanofiber separator. In the wavenumber range of 4000-600 cm^{-1}, PAN/CA nanofiber separators before and after hydrolysis treatment were characterized by FTIR-ATR (Thermo Scientific Nicolet 6700) to analyze the chemical compositions. The contact angles of different separators with distilled water and liquid electrolyte were tested by contact angle goniometer (SL200B,

Solon Tech). The pore size of membrane was analyzed with the Capillary Flow porometer (ipore-1500AEX-Clanp, Porous Materials Inc).

The porosity of separator could be measured by the following Eq (1):

$$\text{Porosity}(\%) = \frac{M_w - m_d}{\rho \times V} \times 100\% \qquad (1)$$

Where M_w and m_d represent the wet weight of separator soaked in n-butanol for an hour and the dry weight of separator, respectively. And ρ represents the density of n-butanol, V represents the volume of the separator.

And the electrolyte uptake could be examined by weighing the mass of separator after immersing in the electrolyte for an hour, and it is calculated according to Eq (2):

$$\text{Electrolyte uptake}(\%) = \frac{M_w - M_d}{M_d} \times 100\% \qquad (2)$$

Where M_w represents the mass of separator after fully absorbing electrolyte, and M_d represents the mass of pristine separator.

After heated at 130 ℃, 150 ℃ for 30 minutes in a preheated air-dried oven, respectively, the thermal stability could be compared directly according to the dimensional shrinkage of different separators. Thermogravimetric analysis (TGA, NETZSCH TA) of separators were performed under N_2 atmosphere at a heating rate of 10 ℃ min^{-1} from 30 ℃ to 600 ℃.

2.5 Electrochemical performance test and battery performance test

The ionic conductivities of PAN and PAN/CA separators were measured via electrochemical impedance spectroscopy (EIS) [57] with a frequency range and AC amplitude of 100 mHz - 100 kHz and 10 mV, respectively. It was calculated using following Eq (3):

$$\sigma = \frac{d}{R_b \times S}$$

(3)

Solon Tech). The pore size of membrane was analyzed with the Capillary Flow porometer (ipore-1500AEX-Clanp, Porous Materials Inc).

Where σ represents the ionic conductivity, d represents the thickness of different separators, S represents actual area of the stainless steel (SS) electrode, R_b represents the bulk resistance.

In order to further measure the lithium ions transport performance in the porous separator, the symmetrical cell of Li/separator/Li was assembled for the potentiometric polarization measurement and EIS. Among which, the test model was subjected to a small DC polarization potential for 1200 s to reach a steady-state current, and corresponding Nyquist plots were measured ranging from 100 mHz to 100 kHz before and after polarization. Then, the t_{Li^+} could be calculated with the following Eq (4) [58]:

$$t^{Li^+} = \frac{I_s(\Delta V - I_0 R_0)}{I_0(\Delta V - I_s R_s)} \qquad (4)$$

Where I_s and I_0 represent the steady-state current and initial current of the obtained I-t curves, respectively. R_s and R_0 represent the interfacial impedance after and before polarization, respectively. And ΔV is the small DC polarization potential (5.0 mV).

The electrochemical stability of the separators was evaluated by linear sweep voltammetry (LSV) using the electrochemical workstation (Solartron 1287, USA) from 3 to 6.5 V (vs. Li^+/Li) at a scanning rate of 5 mV s^{-1} with SS/separator/Li cells.

Coin-type cell (CR-2032) was assembled to evaluate the battery performance with different separators in the Ar-filled glove box (O_2 and H_2O content＜0.01 ppm). The test model consists of a lithium foil as the anode, a commercial $LiCoO_2$ electrode (1.13 cm^2, 11.5 mg cm^{-2}) or $LiFePO_4$ electrode (1.13 cm^2, 11.5 mg cm^{-2}) as the cathode, and a separator soaked with 60 μL electrolyte of 1 M $LiPF_6$ dissolved in EC/DEC (v/v=1/1) containing 5% of FEC. In order to ensure the test system was stable, all assembled cells were placed in argon for 24 h in advance. Cyclic voltammetry (CV) curves were recorded using the electrochemical workstation with the voltage range from 2.5 to 4.5 V and the

scanning rate of 0.1 mV s^{-1}. The EIS data of $LiCoO_2$/Li half cells was measured in the frequency range of 100 mHz-100 kHz. With the charge/discharge voltage ranging from 3.0 V to 4.45 V, cycle performance was studied at a constant charge/discharge current density of 1C. In addition, the C-rate performance was evaluated at various cycling rates from 0.2C to 3C. In the performance characterization section, PE separator was used as the control group.

3. Results and discussions

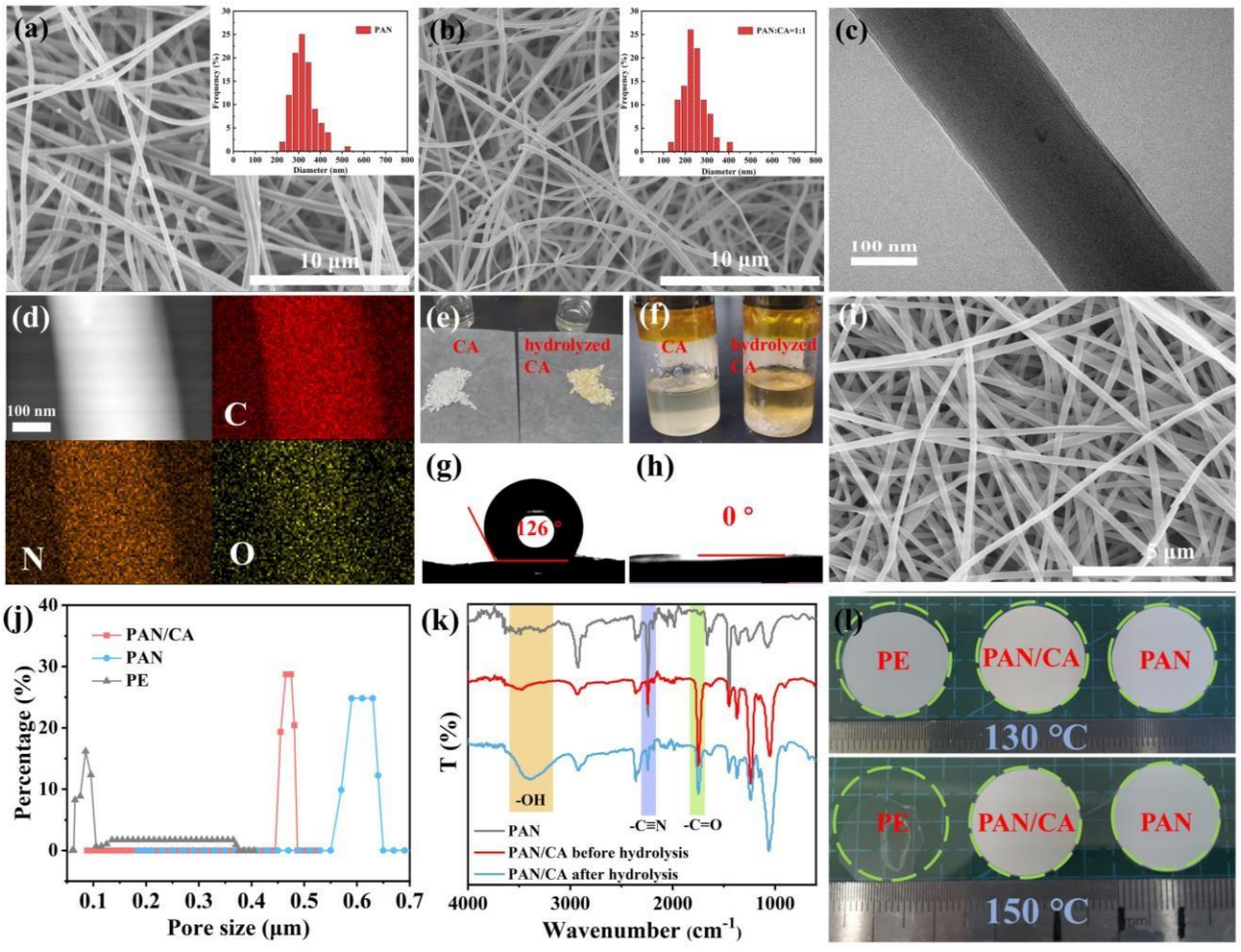

Figure 2. The top-view SEM images and diameter distributions of (a) pure PAN, (b) PAN:CA=1:1. TEM-EDS of pristine PAN/CA nanofiber: (c) TEM image; (d) C, N and O elements mapping images. (e) Optical images of CA before and after alkaline hydrolysis; (f) Optical images of 0.5 g CA and 0.5

g hydrolyzed CA immersed in the liquid electrolyte for 24 h. (g)(h) Contact angels of PAN/CA nanofiber separators before and after alkaline hydrolysis with deionized water, respectively. (i) The top-view SEM image of PAN/CA nanofiber separator after alkaline hydrolysis. (j) Pore size distribution curves of PAN/CA composite nanofiber separator, PAN nanofiber separator and PE separator. (k) FTIR spectra of PAN nanofiber separator and PAN/CA nanofiber separators before and after hydrolysis treatment. (l) The thermal stability test of PE, PAN/CA and PAN separators at 130 ℃ and 150 ℃.

The surface morphology of all prepared nanofiber separator is exhibited in **Figure 2** and **Figure S1**. The original PAN nanofiber separator in **Figure 2(a)** shows a loosely stacked structure among the fibers and its fiber diameter is mainly about 350 nm according to the analysis results of ImageJ software. And the optimal PAN/CA composite nanofiber separator in **Figure 2(b)** obtained from the spinning solution (PAN:CA=1:1) has finer fiber structure and its fiber diameter is about 210 nm, which is expected to improve the electrochemical performance. It is obvious that the nanofiber diameter is able to be decreased with the addition of CA. It is attributed to the fact that CA exhibits better compatibility with the spinning solvent (DMF) and decreases the viscosity of the spinning solution to some extent. So pure CA sample is hard to be fiber in **Figure S1** but is more suitable as the component of PAN co-spun fibers. TEM and energy-dispersive X-ray spectroscopy (EDS) are applied to analyze the C, N and O elements distribution inside the PAN/CA nanofiber and the size of nanofiber. And the corresponding results are shown in **Figure 2(c, d)**, and illustrate that the surface of PAN/CA fiber is flat and smooth. Furthermore, the N element from PAN and the O element of CA are uniformly dispersed in the whole nanofiber, demonstrating that both PAN and CA are mainly components of nanofiber membrane. The mechanical strength of PAN/CA nanofiber separators is enhanced from 3

MPa (PAN) to 11 MPa (**Figure S2**) for denser fiber network structure. And the pore size distribution curves in **Figure 2(j)** also prove that the pore size of PAN/CA nanofiber separator could be decreased for smaller fiber diameter. However, CA is a kind of ester compound and unstable in ester-based electrolyte, and it would be gradually dissolved over time as shown in **Figure 2(e, f)** and **Figure S3.** Herein, a method of alkaline hydrolysis is used to treat these obtained PAN/CA nanofiber separators, which makes partial ester functional groups of CA transform to hydroxyl groups. It could be seen that the color of CA sample will change from white to yellow after alkaline hydrolysis in **Figure 2(e)**. This process can improve the chemical stability of CA in the liquid electrolyte in **Figure 2(f)** and endow CA undissolved for long time by liquid electrolyte.

According to the ATR-FTIR spectra in **Figure 2(k)**, a strong absorption peak at 1750 cm^{-1} is resulted from the C=O group of original PAN/CA nanofiber separator and this absorption peak is significantly reduced after hydrolysis treatment. Moreover, hydrolyzed PAN/CA nanofiber separator would possess a new absorption peak appearing at 3500 cm^{-1} and it is originated from -OH groups. Among these nanofiber separator samples, there is a common absorption peak of the C≡N groups at 2250 cm^{-1}, which is related to the PAN fiber. Additionally, the contact angles are used to distinguish the surface chemical property of these separators with deionized water and liquid electrolyte, respectively. It is easily seen that the contact angle the PAN/CA nanofiber separator with deionized water is decreased from 126° to 0° as depicted in **Figure 2(g, h)** when treated by alkaline solution, revealing an increased hydrophilic property. This result is consistent with the ATR-FTIR spectra that the hydroxyl groups (-OH) are introduced onto the surface of PAN/CA nanofiber separator after hydrolysis treatment. While using liquid electrolyte as the testing liquid (**Figure S4**), all nanofiber separators have the contact angle of 0°, which are smaller than 51.3° of PE separator, illustrating

stronger affinity to liquid electrolyte. Besides, the morphology of PAN/CA nanofiber separator after hydrolysis treatment is provided in **Figure 2(i)**. As expected, this hydrolytic PAN/CA nanofiber separator still maintains a dense and uniform porous structure. In the alkaline hydrolysis process, ester groups of CA are easily hydrolyzed and then transformed to hydroxyl groups and carboxylate acid groups (**Figure 1(b)**). In brief, these results could confirm that the aim of PAN/CA composite nanofiber separator with smaller fiber size and multi-functional groups is achieved, and the hydrolysis process would not damage the original structure of nanofiber.

Thermal stability about separator is a crucial factor determining safety performance of lithium-based batteries, and it is evaluated in **Figure 2(l)**. After holding at 130 °C for 30 minutes, PE separator would appear slight heat shrinkage, while all nanofiber separators still retain the original size. When the temperature is increased to 150 °C exceeding its melting point (136 °C), the porous structure of PE separator would collapse and disappear. In comparison, nanofiber separators have no obvious heat shrinkage and edges curling phenomenon, suggesting that PAN and CA polymer matrix have excellent thermal stability to against dimensional changes. Likewise, TG curves in **Figure S5** also show the thermal stability of these separators. It is noted that PAN and PAN/CA nanofiber separators would not have an obvious mass change before 300 °C, which is already satisfied with the requirement of high-capacity lithium-based battery [59, 60]. And the heat treatment test in **Figure S6** also demonstrates that the PAN/CA composite nanofiber separator could provide a more stable operation voltage.

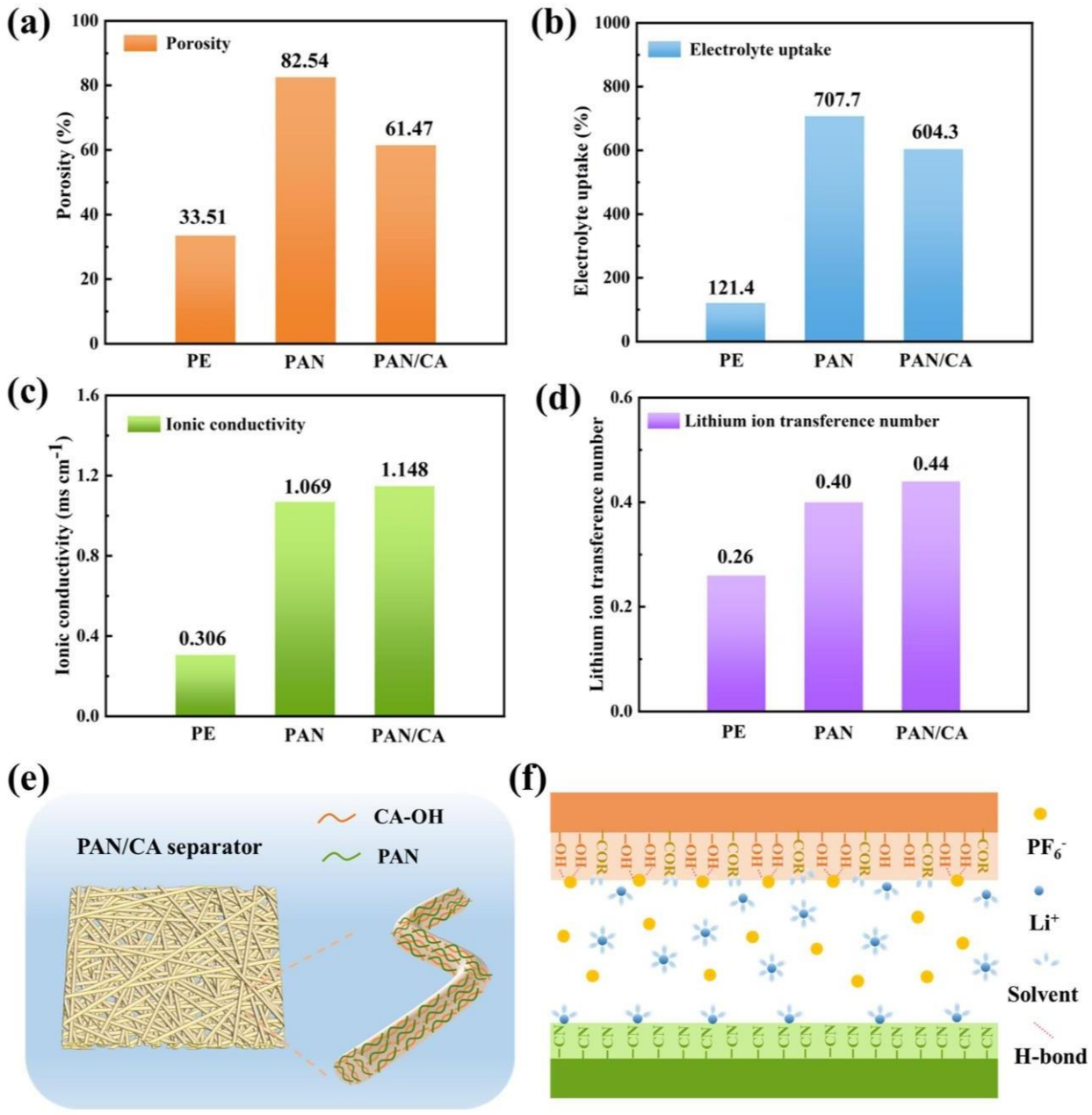

Figure 3. Properties of PE, PAN and PAN/CA separators: (a) porosity; (b) electrolyte uptake; (c) ionic conductivity; (d) lithium-ion transference number. Schematics of (e) PAN/CA nanofiber separator after alkaline hydrolysis and (f) the interaction between the ions in the electrolyte and multi-functional groups on the separators.

In order to investigate porous characteristics of these nanofiber separators, the porosity, electrolyte uptake, ionic conductivity and lithium-ion transference number are tested and the results are shown in **Figure 3**. Commercial PE separator has a porosity of 33.51%, which is lower than 82.54% of PAN nanofiber separator and 61.47% of PAN/CA composite nanofiber separator. Meantime, PE separator also exhibits the lowest electrolyte uptake (121.4%) when compared with these nanofiber separators. It is suggested that the porosity of separator is closely related to electrolyte uptake. In addition, Nyquist plots of the SS/separator/SS blocking cells are given in **Figure S7**, and the X-axis intercept of the diagonal line reflects the bulk impedance (Rb) of blocking cell system, which is used to calculate ionic conductivity of separator filled with liquid electrolyte. As exhibited in **Figure 3(c)**, the hydrolytic PAN/CA composite nanofiber separator has superior ionic conductivity (1.148 mS cm^{-1}) than PAN nanofiber separator and PE separator. Furthermore, we have measured lithium-ion transference number (t_{Li^+}) of all Li-symmetrical cells according to the potentiometric polarization curves and interface impedance before and after polarization (**Figure S8**). As depicted in **Figure 3(d)**, the t_{Li^+} of PAN/CA composite nanofiber separator is 0.44, higher than that of PE (0.26) and PAN separator (0.40), suggesting a better lithium ions transport property of PAN/CA separator. In view of the existence of nitrile groups, ester groups and hydroxyl groups, PAN/CA nanofiber separators have better compatibility with liquid electrolyte. Actual ion transport property is determined by porous structure and surface polarity. This result could be described as the schematics in **Figure 3(e, f)**. It is widely recognized that lithium ions in the liquid electrolyte are wrapped in the solvent molecules, which limits the transportation of lithium ions [61]. Through a simple alkaline hydrolysis reaction, a large number of polar hydroxyl (-OH) groups are generated and dispersed on the surface of PAN/CA composite nanofiber. The polar nitrile groups in PAN would retain a strong interaction with lithium

ions, which accelerates its de-solvation process [52, 53]. And unhydrolyzed ester groups existed in CA could absorb free solvent molecules due to similar polarity. In addition, as one kind of Lewis acid site, the -OH groups could also interact with PF_6^- ions in the liquid electrolyte and form corresponding hydrogen bond, which would restrict the movement of PF_6^- [62-64]. For the synergistic effect of multi-functional groups, free lithium ions in the cells containing PAN/CA nanofiber separators are increased significantly, and then lithium-ion transference number correspondingly gets enhanced.

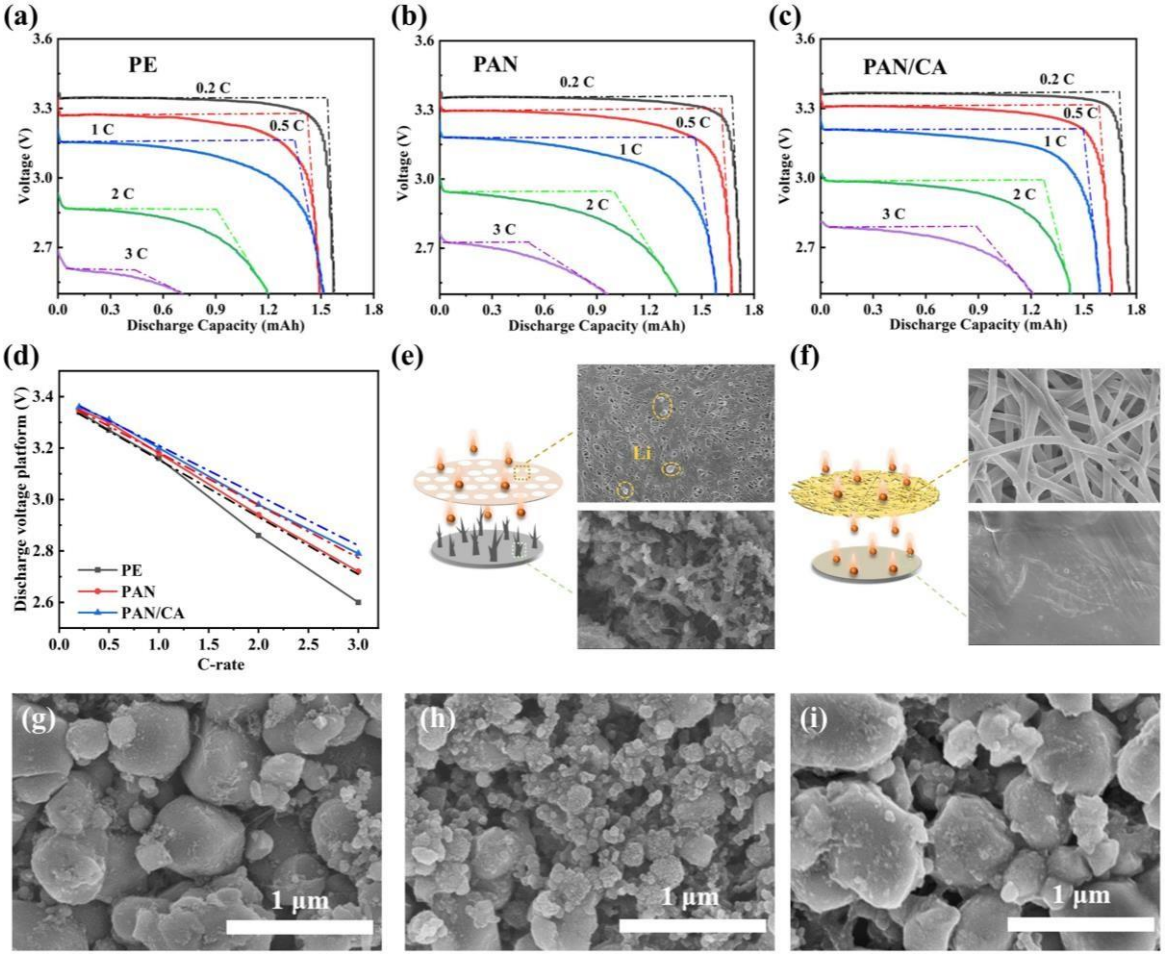

Figure 4. (a-c) Discharge capacity-voltage curves and (d) discharge voltage plateau-rate curve of $LiFePO_4$/Li cells assembled with PE, PAN and PAN/CA separators. The schematics and surface morphology of Li metal anodes and separators from disassembled cells based on (e) PE separators and (f) PAN/CA separators, respectively. The top-view SEM images of (g) pristine $LiFePO_4$ electrodes

and the cycled $LiFePO_4$ electrodes obtained in $LiFePO_4$/Li half cells employing (h) PE separators and (i) PAN/CA composite nanofiber separators.

Considering the stable discharge process and flat discharge voltage plateau, $LiFePO_4$/Li cells are assembled to compare the concentration polarization phenomenon in these cases about PE separator and nanofiber separators, and the plots of discharge capacity-voltage curves under different current density are shown in **Figure 4(a-c)**. It is well-recognized that the relationship of $\Delta E = I(R_s + R_{ct} + R_{W_b} + R_{cp})$ is existed inside the battery, R_s, R_{ct}, R_{W_b} and R_{cp} are the migration impedance of liquid phase, the charge transfer impedance, the diffusion impedance of solid phase and the impedance of concentration polarization, respectively. Therefore, the concentration polarization can be studied by polarization voltage. The plot of corresponding relation between discharge voltage plateau and C-rate is obtained and depicted in **Figure 4(d)**. The dotted line represents the linear relation that the polarization voltage should proportional to the discharge current after fitting, while the solid line represents the true relation for an enhanced concentration polarization effect especially under the condition of high current density. When the current density is lower than 1C, solid line is almost consistent with dotted line. The discharge voltage plateau of cell assembled with PAN/CA separator (3.36 V at 0.2C, 3.31 V at 0.5C, 3.20 V at 1C) is similar with those of PAN separator (3.34 V at 0.2C, 3.30 V at 0.5C, 3.18 V at 1C) and PE separator (3.33 V at 0.2C, 3.27 V at 0.5C, 3.16 V at 1C). However, with the further increase of discharge current density, the discharge voltage plateau of cells assembled with PE and PAN separators are reduced to 2.60 V at 3C and 2.72 V at 3C, respectively. In contrast, cell assembled with PAN/CA separator still possesses a higher discharge plateau of 2.79 V, illustrating that the polarization is smaller than PAN separator and PE separator. Due to the higher t_{Li^+} and ionic

conductivity of PAN/CA separator, the concentration polarization of cell at high current density is significantly alleviated.

Meanwhile, we also explored the stability of these battery parts during the long-term cycles. **Figure S9(a)** shows the $LiFePO_4$/Li cells with PAN/CA nanofiber composite separators exhibit better capacity ability than those cells employing PE separators. Then these cycled cells are opened to evaluate the operation state of all battery parts. The obtained FTIR spectra of PAN/CA separator in **Figure S9(b)** demonstrates that the -OH groups dispersed in the nanofiber could be stably remained inside the cells and facilitate the transport process of lithium ions for long time. **Figure 4(e-f)** and **Figure S10** show the schematics of Li-deposited process and the morphology of PAN/CA separator and PE separator. It could be seen that the PAN/CA nanofiber separator still maintains a dense and uniform porous structure, while PE separator partly presents the blocked porous structure and has some broken "dead Li" for low ionic conduction rate and inhomogeneous lithium-ion flux. As a result, in the case of PAN/CA nanofiber separators, the morphology of lithium anode in **Figure S11(d-f)** has a smoother surface after repeating Li platting/stripping process when compared with original Li foil (**Figure S11(a-c)**). Moreover, as shown in **Figure S11(g-i)**, lithium anode from $LiFePO_4$/Li cell with PE separator has lots of loosely stacked dendritic or rodlike Li metal, which would consume more liquid electrolyte and decrease the cycle life of battery. As exhibited in **Figure 4(g-i)** and **Figure S12**, the $LiFePO_4$ electrode from the cell with PAN/CA separator is composed of even-distributed bulk active materials with a smooth surface, is more like original electrode. While the $LiFePO_4$ particles of PE separator are hard to maintain the structure stability and covered with many tiny by-products, which might hinder the electrochemical reaction kinetics and degrade the battery performance. Therefore, the

efficient ionic conduction ability of PAN/CA nanofiber separators can guarantee the stability of electrodes and correspondingly alleviate the internal polarization of cells.

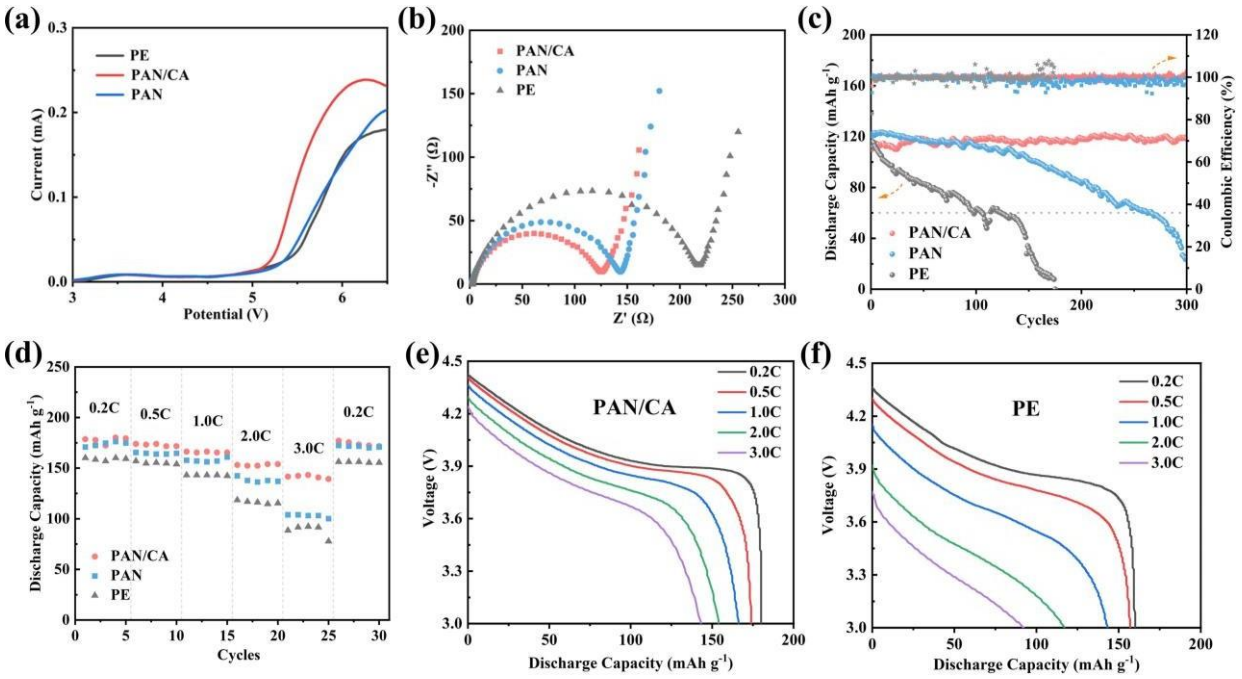

Figure 5. (a) Linear sweep voltammetry (LSV) curves of Li/SS cells with PAN/CA, PAN and PE separators; (b) Nyquist plots of the $LiCoO_2$/Li cells with PAN/CA, PAN and PE separators. (c) Long-term cycle performance of $LiCoO_2$/Li cells based on PAN/CA, PAN and PE separators. (d) Rate performance of $LiCoO_2$/Li cells with PAN/CA, PAN and PE separators. (e)(f) Discharge capacity-voltage curves of $LiCoO_2$/Li cells assembled with PAN/CA nanofiber separators and PE separators, respectively.

Other electrochemical performance of separators is discussed in **Figure 5**. According to the LSV curves in **Figure 5(a)**, there is a similar shape of LSV curves in three separators. And there is no obvious polarization current of these test systems until the voltage of 5 V, which indicates that electrospinning nanofiber separator with excellent electrochemical stability could fully satisfy the demand of common lithium-ion battery application (2.5-4.5 V). In another case of $LiCoO_2$/Li cells,

there are an obvious oxidation peak and a reduction peak on the CV curve (**Figure S13**), which corresponds to the process of insert-lithium and de-lithium of cathode, and it illustrates good cyclic reversibility of PAN/CA nanofiber separator. **Figure 5(b)** shows the Nyquist plots of $LiCoO_2$/Li cells based on different separators. The whole curve reflects the impedance of ions during the transport process inside the porous separator and at the electrode/electrolyte interface. During the intermediate frequency region, the semi-circular arc represents the charge transfer impedance related to electrochemical polarization, which could reflect the compatibility between the electrode and the separator interface. Compared with 220 Ω of PE separator and 150 Ω of pure PAN nanofiber separator, it is obvious that PAN/CA composite nanofiber separator has a comparatively smaller interface impedance (120 Ω). This result is mainly attributed to the enhancement of the liquid electrolyte uptake and the introduction of surface polar functional groups in PAN/CA separator, which is beneficial to battery performance. **Figure 5(c)** displays the battery discharge capacity and coulombic efficiency at a constant current density of 1C. Obviously, the cells with PAN/CA nanofiber separator possess great cycle performance and still remain the discharge capacity of 118.5 mAh g^{-1} even after 300 cycles. It is resulted from the fact that the PAN/CA separators possess outstanding affinity to the liquid electrolyte and great interface stability. In addition, abundant -OH functional groups dispersed in the PAN/CA nanofiber could regulate lithium-ion flux and form a stable solid electrolyte interface (SEI). In contrast, owing to the rapid consumption of liquid electrolyte, the discharge capacity of the cells based on PE separator decayed quickly to below 60 mAh g^{-1} after 100 cycles. According to the plots of capacity vs. voltage in **Figure S14**, $LiCoO_2$/Li half cells assembled with PAN/CA nanofiber separators also demonstrate a better capacity retention ratio. Besides, battery rate performance is exhibited in **Figure 5(d)**, which corresponds the plots of discharge capacity vs. voltage in **Figure 5(e)(f)** and **Figure S15**.

It is clear that the capacity of the cells with PAN/CA and PAN nanofiber separator is higher than that of cells based on PE separators at a small discharge current density. It is attributed to the reason that nanofiber separators have higher porosity and electrolyte uptake. As the current density is increased to 3C, the cells assembled with PAN/CA nanofiber separators still possess a capacity retention of 79.5% (143.1 mAh g^{-1}), which is better than that of PE separators (57.1%, 92.3 mAh g^{-1}) and PAN separators (59.2%, 103.9 mAh g^{-1}). These results indicate that PAN/CA separators with multi-functional groups have a better retention ability for liquid electrolyte, which is particularly important to the issue of solvent consuming at high current density. In addition, a more efficient process for transporting lithium ions alleviates the phenomenon of concentration polarization inside the cells. Similarly, the rate performance (**Figure S16**) of $LiFeO_4$/Li half cells also demonstrates this result.

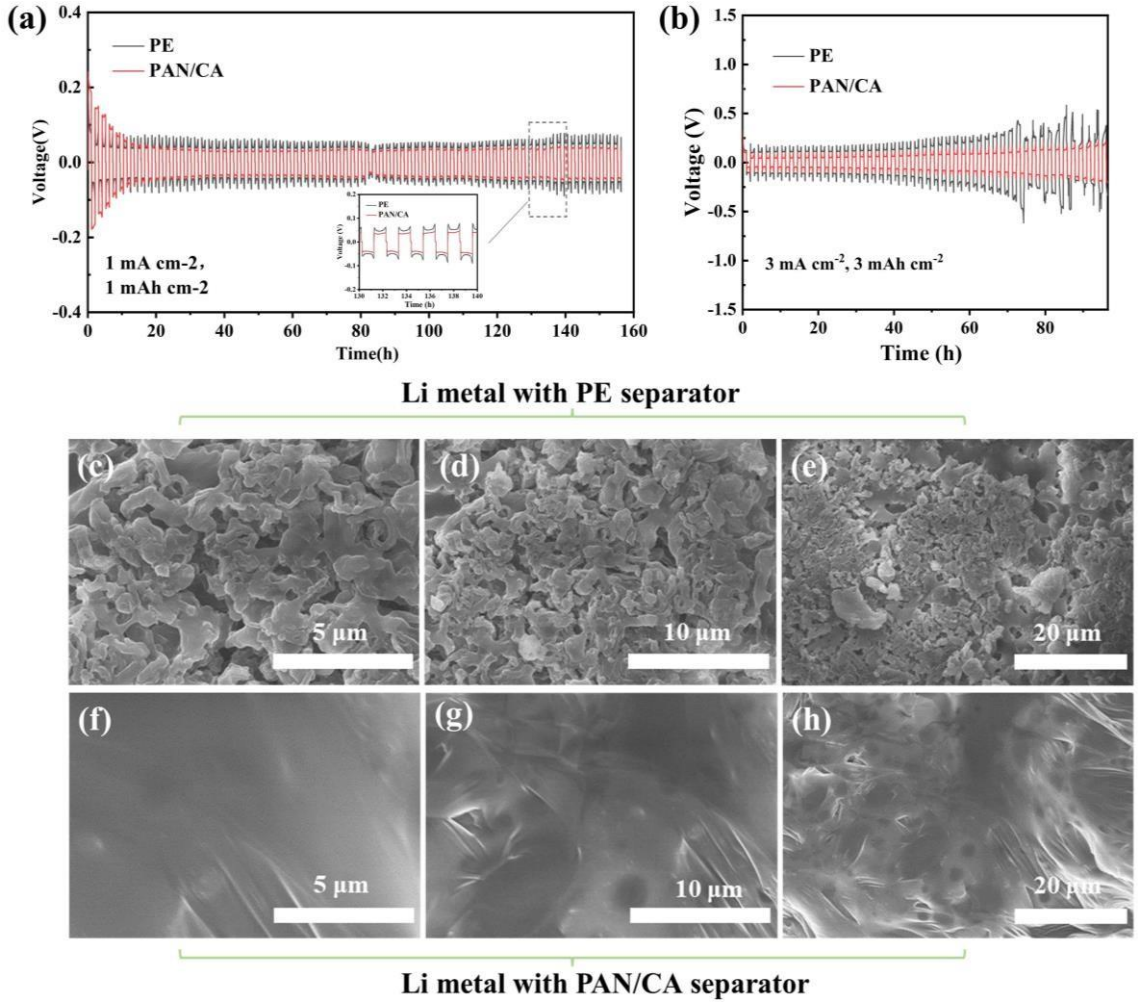

Figure 6. Charge-discharge voltage-time profiles of Li-symmetrical cells assembled with PE separator and PAN/CA nanofiber separator at (a) 1 mA cm^{-2} for 1mAh cm^{-2} and (b) 3 mA cm^{-2} for 3mAh cm^{-2}. The top-view SEM images of Li metal anodes from Li-symmetrical cells assembled with (c-e) PE separators and (f-h) PAN/CA nanofiber separators after long-term Li platting/stripping process.

Furthermore, the cycling stability of Li-symmetrical cells are operated to further explore interfacial electrochemical stability of Li anode/separators. As expected, the Li-symmetrical cells with PAN/CA separators deliver lower overpotential than that of PE separators during the Li plating/stripping process (the current density of 1.0 mA cm^{-2}, the areal capacity of 1 mAh cm^{-2}) in **Figure 6(a)**, indicating a lower polarization status and a better cycle stability. After disassembling

these cells, it is found the surface of Li anode from the symmetric cells equipped with PAN/CA separators (**Figure 6(f-h)**) is relatively smooth, while a large quantity of dendritic and rod-like deposition is observed on the surface of control group (**Figure 6(c-e)**). As the current density is increased, the Li-symmetrical cells with PAN/CA separators still maintain a more stable cycle state (**Figure 6(b)** and **Figure S17**). These results confirm that the functional PAN/CA composite nanofiber separators with excellent interface compatibility and high-efficiency lithium ions transport ability could contribute to constructing a more stable Li metal anode. As is known to all, the battery performance is closely related to the test conditions, such as the environment temperature, charge-discharge current density, the active materials loading of cathode and so on. Compared with other polymer separators prepared by electrospinning or phase separation recently reported in the literature, the PAN/CA composite nanofiber separator exhibits equivalent (even better) ionic conduction ability and capacity retention rate (**Table S1**). In brief, the PAN/CA composite nanofiber separators prepared by electrospinning and dissociation treatment could be applicated into lithium-based batteries with high energy density.

4. Conclusion

In this study, we have successfully prepared a kind of surface functionalized PAN/CA composite nanofiber separator with multi-functional groups. On the one hand, the PAN/CA separator shows excellent thermal stability at 150 °C, which could guarantee the high temperature safety performance of the battery. On the other hand, the existence of -OH groups, -CN groups and ester groups improve the surface polarity of PAN/CA nanofiber separator, and high porosity correspondingly enhances the electrolyte uptake of separator. It is demonstrated that the interactions such as hydrogen bonding and

intermolecular forces among multi-functional groups, solvent and ions can promote selective transport of Li^+. Thus, the $LiCoO_2$/Li cells with PAN/CA composite nanofiber separator have stable and excellent cycle performance for its excellent lithium-ion migration ability. Even at the high current density of 3C, the cells still possess a discharge capacity of 143.1 mAh g^{-1}. These results suggest PAN/CA separator with multi-functional groups is a potential for next-generation lithium-based batteries.

ASSOCIATED CONTENT

Supporting Information available:

Figure S1. SEM images; **Figure S2**. Stress-strain curves; **Figure S3.** Stability test of CA and alkaline hydrolyzed CA; **Figure S4.** Contact angels; **Figure S5.** TGA curves; **Figure S6.** Voltage profiles. **Figure S7.** Nyquist plots; **Figure S8.** Steady-state current curves and the Nyquist plots before and after polarization; **Figure S9.** Cycle performance and FTIR spectra; **Figure S10-S12.** SEM images; **Figure S13.** CV curves; **Figure S14.** Capacity-voltage curves; **Figure S15.** Discharge Capacity-voltage curve; **Figure S16.** Rate performance; **Figure S17.** Charge-discharge voltage-time profiles; **Table S1.** Performance comparison; **Table S2.** Physical properties.

Acknowledgements

This work was supported by Fundamental Research Funds for the Central Universities (NE2018104), National Natural Science Foundation of China (11575084) and A Project Funded by the Priority Academic Program Development of Jiangsu Higher Education Institutions (PAPD).

Reference

[1] G. Jeong, Y. Kim, H. Kim, Y. Kim, H. Sohn, Prospective materials and applications for Li secondary batteries, Energ. Environ. Sci. 4 (2011) 1986, https://doi.org/10.1039/c0ee00831a

[2] T. Takamura, Trends in Advanced Batteries and Key Materials in the New Century, Solid State Ionics, 152-153(2002) 19-34, https://doi.org/10.1016/S0167-2738(02)00325-9

[3] M.R. Palacín, Recent advances in rechargeable battery materials: a chemist's perspective, Chem. Soc. Rev. 38 (2009) 2565, https://doi.org/10.1039/b820555

[4] H. Gong, T. Wang, K. Chang, P. Li, L. Liu, X. Yu, B. Gao, H. Xue, R. Ma, J. He, J. Ye, Revealing the illumination effect on the discharge products in high- performance Li–O_2 batteries with heterostructured photocatalysts. Carbon Energy (2022), https://doi.org/10.1002/cey2.208

[5] P. Arora, Z.J. Zhang, Battery Separators. Chem. Rev. 104 (2004) 4419-4462, https://doi.org/ 10.1002/adma.200800627

[6] Y. Guo, J. Hu, L. Wan, Nanostructured Materials for Electrochemical Energy Conversion and Storage Devices. Adv. Mater. 20 (2008) 2878-2887, https://doi.org/10.1002/adma.200800627

[7] H. Lee, M. Yanilmaz, O. Toprakci, K. Fu, X. Zhang, A review of recent developments in membrane separators for rechargeable lithium-ion batteries, Energ. Environ. Sci. 7 (2014) 3857-3886, https://doi.org/10.1039/c4ee01432d

[8] H. Li, Z. Wang, L. Chen, X. Huang, Research on Advanced Materials for Li-ion Batteries, Adv. Mater. 21 (2009) 4593-4607, https://doi.org/10.1002/adma.200901710

[9] K.A. Severson, P.M. Attia, N. Jin, N. Perkins, B. Jiang, Z. Yang, M.H. Chen, M. Aykol, P.K. Herring, D. Fraggedakis, M.Z. Bazant, S.J. Harris, W.C. Chueh, R.D. Braatz, Data-driven prediction of battery cycle life before capacity degradation, Nat. Energy 4 (2019) 383-391,

https://doi.org/10.1038/s41560-019-0356-8

[10] Q. Wang, Z. Yao, C. Zhao, T. Verhallen, D.P. Tabor, M. Liu, F. Ooms, F. Kang, A. Aspuru-Guzik, Y. Hu, M. Wagemaker, B. Li, Interface chemistry of an amide electrolyte for highly reversible lithium metal batteries, Nat. Commun. 11 (2020), https://doi.org/10.1038/s41467-020-17976-x

[11] M. Li, L. Sheng, H. Zhang, Y. Yang, R. Xu, Y. Bai, S. Song, G. Liu, T. Wang, X. Huang, J. He, Effect of the heat treatment temperature on mechanical and electrochemical properties of polyimide separator for lithium ion batteries, J. Mater. Sci. 55 (2020) 16158-16170, https://doi.org/10.1007/s10853-020-05197-y

[12] S. Jia, J. Long, J. Li, S. Yang, K. Huang, N. Yang, Y. Liang, J. Xiao, Biomineralized zircon-coated PVDF nanofiber separator for enhancing thermo- and electro-chemical properties of lithium ion batteries, J. Mater. Sci. 55 (2020) 14907-14921, https://doi.org/10.1007/s10853-020-05051-1

[13] L. Fu, A. Xu, Y. Song, J. Ju, H. Sun, Y. Yan, and S. Wu, Pinecone-like Silicon@Carbon Microspheres Covered by Al_2O_3 nano-petals for lithium-ion battery anode under high temperature. Electrochim. Acta 387 (2021) 138461, https://doi.org/10.1016/j.electacta.2021.138461

[14] L. Xue, Q. Zhang, Y. Huang, H. Zhu, L. Xu, S. Guo, X. Zhu, H. Liu, Y. Huang, J. Huang, L. Lu, S. Zhang, L. Gu, Q. Liu, J. Zhu, H. Xia, Stabilizing Layered Structure in Aqueous Electrolyte via Dynamic Water Intercalation/Deintercalation. Adv. Mater., 34 (2022) 2108541, https://doi.org/10.1002/adma.202108541

[15] L. Xue, Q. Zhang, X. Zhu, L. Gu, J. Yue, Q. Xia, T. Xing, T. Chen, Y. Yao, and H. Xia, 3D

$LiCoO_2$ nanosheets assembled nanorod arrays via confined dissolution-recrystallization for advanced aqueous lithium-ion batteries. Nano Energy 56 (2019) 463-472, https://doi.org/10.1016/j.nanoen.2018.11.085

[16] Q. Xia, M. Ni, M. Chen, and H. Xia, Low-temperature synthesized self-supported single-crystalline $LiCoO_2$ nanoflake arrays as advanced 3D cathodes for flexible lithium-ion batteries. J. Mater. Chem. A 7 (2019) 6187-6196, https://doi.org/10.1039/C9TA00351G

[17] C.F.J. Francis, I.L. Kyratzis, A.S. Best, Lithium- Ion Battery Separators for Ionic- Liquid Electrolytes: A Review, Adv. Mater. 32 (2020) 1904205, https://doi.org/10.1002/adma.201904205

[18] S.S. Zhang, A review on the separators of liquid electrolyte Li-ion batteries, J. Power Sources 164 (2007) 351-364, https://doi.org/10.1016/j.jpowsour.2006.10.065

[19] M.R. Asghar, M.T. Anwar, A. Naveed, J. Zhang, A Review on Inorganic Nanoparticles Modified Composite Membranes for Lithium-Ion Batteries: Recent Progress and Prospects, Membranes 9 (2019) 78, https://doi.org/10.3390/membranes9070078

[20] R. Zahn, M.F. Lagadec, V. Wood, Transport in Lithium Ion Batteries: Reconciling Impedance and Structural Analysis, ACS Energy Letters 2 (2017) 2452-2453, https://doi.org/10.1021/acsenergylett.7b00740

[21] X. Huang, Separator technologies for lithium-ion batteries, J. Solid State Electr. 15 (2011) 649-662, https://doi.org/10.1007/s10008-010-1264-9

[22] H. Liao, H. Hong, H. Zhang, Z. Li, Preparation of hydrophilic polyethylene/methylcellulose blend microporous membranes for separator of lithium-ion batteries, J. Membrane Sci. 498 (2016) 147-157, https://doi.org/10.1016/j.memsci.2015.09.064

[23] E. Wang, H. Wu, C. Chiu, P. Chou, The Effect of Battery Separator Properties on Thermal Ramp, Overcharge and Short Circuiting of Rechargeable Li-Ion Batteries, J. Electrochem. Soc. 166 (2019) A125-A131, https://doi.org/10.1149/2.0381902jes

[24] L. Sheng, L. Wang, J. Wang, H. Xu, X. He, Accelerated lithium-ion conduction in covalent organic frameworks. Chem. Commun. 56 (2020) 10465-10468, https://doi.org/10.1039/D0CC04324A

[25] M. Yuan, K. Liu, Rational design on separators and liquid electrolytes for safer lithium-ion batteries, J. Energy Chem. 43 (2020) 58-70, https://doi.org/10.1016/j.jechem.2019.08.008

[26] C. Karuppiah, Y. Hsieh, S.L. Beshahwured, X. Wu, S. Wu, R. Jose, S.J. Lue, C. Yang, Poly(vinyl alcohol)/Melamine Composite Containing LATP Nanocrystals as a High-Performing Nanofibrous Membrane Separator for High-Power, High-Voltage Lithium-Ion Batteries, ACS Applied Energy Materials 3 (2020) 8487-8499, https://doi.org/10.1021/acsaem.0c01132

[27] J. Park, J. Cho, W. Park, D. Ryoo, S. Yoon, J.H. Kim, Y.U. Jeong, S. Lee, Close-packed SiO_2/poly(methyl methacrylate) binary nanoparticles-coated polyethylene separators for lithium-ion batteries, J. Power Sources 195 (2010) 8306-8310, https://doi.org/10.1016/j.jpowsour.2010.06.112

[28] J. Cho, Y. Jung, Y.S. Lee, D. Kim, High performance separator coated with amino-functionalized SiO_2 particles for safety enhanced lithium-ion batteries, J. Membrane Sci. 535 (2017) 151-157, https://doi.org/10.1016/j.memsci.2017.04.042

[29] Y.B. Kim, T. Tran-Phu, M. Kim, D. Jung, G. Yi, J.H. Park, Facilitated Ion Diffusion in Multiscale Porous Particles: Application in Battery Separators, ACS Appl. Mater. Inter. 7 (2015) 4511-4517, https://doi.org/10.1021/am506797d

[30] S. Oh, J.K. Lee, D. Byun, W.I. Cho, B. Won Cho, Effect of Al_2O_3 coating on electrochemical performance of $LiCoO_2$ as cathode materials for secondary lithium batteries, J. Power Sources 132 (2004) 249-255, https://doi.org/10.1016/j.jpowsour.2004.01.049

[31] D. Lee, S. Lee, Y. Kim, J. Oh, Preparation of a high-purity ultrafine α-Al_2O_3 powder and characterization of an Al_2O_3-coated PE separator for lithium-ion batteries, Powder Technol, 320 (2017) 125-132, https://doi.org/10.1016/j.powtec.2017.07.027

[32] J. Choi, S.H. Kim, D. Kim, Enhancement of thermal stability and cycling performance in lithium-ion cells through the use of ceramic-coated separators, J. Power Sources 195 (2010) 6192-6196, https://doi.org/10.1016/j.jpowsour.2009.11.020

[33] X. Wang, H. Hua, L. Peng, B. Huang, P. Zhang, J. Zhao, Functional separator for promoting lithium ion migration and its mechanism study, Appl. Surf. Sci. 542 (2021) 148661, https://doi.org/10.1016/j.apsusc.2020.148661

[34] K. Peng, B. Wang, Y. Li, C. Ji, Magnetron sputtering deposition of TiO_2 particles on polypropylene separators for lithium-ion batteries, RSC Adv. 5 (2015) 81468-81473, https://doi.org/10.1039/c5ra18171b

[35] L. Liu, Y. Wang, C. Gao, C. Yang, K. Wang, H. Li, H. Gu, Ultrathin ZrO_2-coated separators based on surface sol-gel process for advanced lithium ion batteries, J. Membrane Sci. 592 (2019) 117368, https://doi.org/10.1016/j.memsci.2019.117368

[36] J. Liang, Q. Chen, X. Liao, P. Yao, B. Zhu, G. Lv, X. Wang, X. Chen, J. Zhu, A Nano- shield Design for Separators to Resist Dendrite Formation in Lithium- Metal Batteries, Angewandte Chemie International Edition 59 (2020) 6561-6566, https://doi.org/10.1002 /anie.201915440

[37] J. Shi, Y. Xia, S. Han, L. Fang, M. Pan, X. Xu, Z. Liu, Lithium ion conductive

$Li_{1.5}Al_{0.5}Ge_{1.5}(PO_4)_3$ based inorganic–organic composite separator with enhanced thermal stability and excellent electrochemical performances in 5 V lithium ion batteries, J. Power Sources, 273(2015) 389-395, https://doi.org/10.1016/j.jpowsour.2014.09.105

[38] Y. Wang, S. Wang, J. Fang, L. Ding, H. Wang, A nano-silica modified polyimide nanofiber separator with enhanced thermal and wetting properties for high safety lithium-ion batteries, J. Membrane Sci. 537 (2017) 248-254, https://doi.org/10.1016/j.jpowsour.2005.10.104

[39] X. Shi, Q. Sun, B. Boateng, Y. Niu, Y. Han, W. Lv, W. He, A quasi-solid composite separator with high ductility for safe and high-performance lithium-ion batteries, J. Power Sources 414 (2019) 225-232, https://doi.org/10.1016/j.jpowsour.2019.01.005

[40] C.Z. Zhao, P.Y. Chen, R. Zhang, X. Chen, B.Q. Li, X.Q. Zhang, X.B. Cheng, Q. Zhang, An ion redistributor for dendrite-free lithium metal anodes, Sci Adv, 4 (2018) t3446, https://doi.org/10.1126/sciadv.aat3446

[41] Y. Wang, S. Wang, J. Fang, L. Ding, H. Wang, A nano-silica modified polyimide nanofiber separator with enhanced thermal and wetting properties for high safety lithium-ion batteries, J. Membrane Sci, 537 (2017) 248-254, https://doi.org/10.1016/j.memsci.2017.05.023

[42] Y. Miao, G. Zhu, H. Hou, Y. Xia, T. Liu, Electrospun polyimide nanofiber-based nonwoven separators for lithium-ion batteries, J. Power Sources 226 (2013) 82-86, https://doi.org/10.1016/j.jpowsour.2012.10.027

[43] Y. Choi, K. Zhang, K.Y. Chung, D.H. Wang, J.H. Park, PVdF-HFP/exfoliated graphene oxide nanosheet hybrid separators for thermally stable Li-ion batteries, Rsc Adv. 6 (2016) 80706-80711, https://doi.org/10.1039/C6RA15062D

[44] C. Yang, Z. Jia, Z. Guan, L. Wang, Polyvinylidene fluoride membrane by novel electrospinning

system for separator of Li-ion batteries, J. Power Sources 189 (2009) 716-720, https://doi.org/10.1016/j.jpowsour.2008.08.060

[45] J. Cui, J. Liu, C. He, J. Li, X. Wu, Composite of polyvinylidene fluoride–cellulose acetate with $Al(OH)_3$ as a separator for high-performance lithium ion battery, J. Membrane Sci. 541 (2017) 661-667, https://doi.org/10.1016/j.memsci.2017.07.048

[46] L. Wang, F. Liu, W. Shao, S. Cui, Y. Zhao, Y. Zhou, J. He, Graphite oxide dopping polyimide nanofiber membrane via electrospinning for high performance lithium-ion batteries, Composites Communications 16 (2019) 150-157, https://doi.org/10.1016/j.coco.2019.09.004

[47] D. Wu, N. Dong, R. Wang, S. Qi, B. Liu, D. Wu, In situ construction of High-safety and Non-flammable polyimide "Ceramic" Lithium-ion battery separator via SiO_2 Nano-Encapsulation, Chem. Eng. J., 420 (2021) 129992, https://doi.org/10.1016/j.cej.2021.129992

[48] M. Yanilmaz, Y. Lu, J. Zhu, X. Zhang, Silica/polyacrylonitrile hybrid nanofiber membrane separators via sol-gel and electrospinning techniques for lithium-ion batteries, J. Power Sources 313 (2016) 205-212, https://doi.org/10.1016/j.jpowsour.2016.02.089

[49] T. Cho, M. Tanaka, H. Onishi, Y. Kondo, T. Nakamura, H. Yamazaki, S. Tanase, T. Sakai, Battery performances and thermal stability of polyacrylonitrile nano-fiber-based nonwoven separators for Li-ion battery, J. Power Sources 181(2008) 155-160, https://doi.org/10.1016/j.jpowsour.2008.03.010

[50] Y. Kim, H. Kim, C. Doh, S.H. Kim, S. Lee, Technological potential and issues of polyacrylonitrile based nanofiber non-woven separator for Li-ion rechargeable batteries, J. Power Sources 244 (2013) 196-206, https://doi.org/10.1016/j.jpowsour.2013.01.166

[51] S. Park, Y. Jung, W. Shin, K.H. Ahn, C.H. Lee, D. Kim, Cross-linked fibrous composite

separator for high performance lithium-ion batteries with enhanced safety, J. Membrane Sci. 527 (2017) 129-136, https://doi.org/10.1016/j.memsci.2017.01.015

[52] X. Ma, P. Kolla, R. Yang, Z. Wang, Y. Zhao, A.L. Smirnova, H. Fong, Electrospun polyacrylonitrile nanofibrous membranes with varied fiber diameters and different membrane porosities as lithium-ion battery separators, Electrochim. Acta 236 (2017) 417-423, https://doi.org/ 10.1016/j.electacta.2017.03.205

[53] G. Zainab, X. Wang, J. Yu, Y. Zhai, A. Ahmed Babar, K. Xiao, B. Ding, Electrospun polyacrylonitrile/polyurethane composite nanofibrous separator with electrochemical performance for high power lithium ion batteries, Mater. Chem. Phys. 182 (2016) 308-314, https://doi.org/ 10.1016/j.matchemphys.2016.07.037

[54] E.M. Çanga, and F.C. Dudak, Improved digestive stability of probiotics encapsulated within poly(vinyl alcohol)/cellulose acetate hybrid fibers, Carbohyd. Polym. 264 (2021) 117990, https://doi.org/10.1016/j.carbpol.2021.117990

[55] J. Hu, Y. Liu, M. Zhang, J. He, P. Ni, A separator based on cross-linked nano-SiO_2 and cellulose acetate for lithium-ion batteries, Electrochim. Acta 334 (2020) 135585, https://doi.org/ 10.1016/j.electacta.2019.135585

[56] J. Liu, W. Li, X. Zuo, S. Liu, Z. Li, Polyethylene-supported polyvinylidene fluoride–cellulose acetate butyrate blended polymer electrolyte for lithium ion battery, J. Power Sources 226 (2013) 101-106, https://doi.org/10.1016/j.jpowsour.2012.10.078

[57] H. Zhang, L. Sheng, Y. Bai, S. Song, G. Liu, H. Xue, T. Wang, X. Huang, J. He, Amino-Functionalized Al_2O_3 Particles Coating Separator with Excellent Lithium- Ion Transport Properties for High- Power Density Lithium- Ion Batteries, Adv. Eng. Mater. 22 (2020)

1901545, https://doi.org/10.1002/adem.201901545

[58] Q. Du, M. Yang, J. Yang, P. Zhang, J. Qi, L. Bai, Z. Li, J. Chen, R. Liu, X. Feng, Z. Huang, T. Masese, Y. Ma, W. Huang, Bendable Network Built with Ultralong Silica Nanowires as a Stable Separator for High-Safety and High-Power Lithium-Metal Batteries, ACS Appl. Mater. Inter. 11 (2019) 34895-34903, https://doi.org/10.1021/acsami.9b09722

[59] H. Chen, X. Jiao, Preparation and characterization of Polyvinylidene fluoride/Octaphenyl-Polyhedral oligomeric silsesquioxane hybrid Lithium-ion battery separators by electrospinning, Solid State Ionics 310 (2017) 134-142, https://doi.org/10.1016/j.ssi.2017.08.017

[60] L. Li, P. Liu, Q.S. Fu, Y. Gong, S.R. Zhang, H.J. He, J. Chen, Study on preparation of polyacrylonitrile/polyimide composite lithium-ion battery separator by electrospinning, J. Mater. Res. 34 (2019) 642-651, https://doi.org/10.1557/jmr.2019.8

[61] L. Sheng, L. Song, H. Gong, J. Pan, Y. Bai, S. Song, G. Liu, T. Wang, X. Huang, J. He, Polyethylene separator grafting with polar monomer for enhancing the lithium-ion transport property, J. Power Sources 479 (2020) 228812, https://doi.org/10.1016/j.jpowsour.2020.228812

[62] C. Lin, H. Zhang, Y. Song, Y. Zhang, J. Yuan, B. Zhu, Carboxylated polyimide separator with excellent lithium ion transport properties for a high-power density lithium-ion battery, J. Mater. Chem. A 6 (2018) 991-998, https://doi.org/10.1039/C7TA08702K

[63] W. Fu, R. Xu, X. Zhang, Z. Tian, H. Huang, J. Xie, C. Lei, Enhanced wettability and electrochemical performance of separators for lithium-ion batteries by coating core-shell structured silica-poly(cyclotriphosphazene-co-4,4′-sulfonyldiphenol) particles, J. Power Sources 436 (2019) 226839, https://doi.org/10.1016/j.jpowsour.2019.226839

[64] J. Zhang, X. Huang, H. Wei, J. Fu, Y. Huang, X. Tang, Enhanced electrochemical properties of

polyethylene oxide-based composite solid polymer electrolytes with porous inorganic–organic hybrid polyphosphazene nanotubes as fillers, J. Solid State Electr. 16 (2012) 101-107, https://doi.org/10.1007/s10008-010-1278-3